Numerical study on the effect of leading-edge tubercle on symmetrical airfoil at low Reynolds number

Jeena Joseph[1] Sathyabhama A[2]

[1] Research Scholar, Department of Mechanical Engineering, NITK Surathkal, Mangalore 575025, Karnataka, India
Me16f05.jeena@nitk.edu.in,jeenajoseph@live.in

[2] Associate Professor, Department of Mechanical Engineering, NITK Surathkal, Mangalore 575025, Karnataka, India
Bhama72@gmail.com

Abstract. The protrusions known as tubercle on the leading edge of a humpback whale flipper help in the maneuverability of the whale despite its huge size. This work is computational study of stall characteristics as well as the flow pattern on NACA 0021 airfoil with leading edge tubercle as well as normal airfoil at a low Reynolds number of 100 000. SST $k-\omega$ turbulence model based on unsteady RANS scheme is used to model the flow over airfoils at different angles of attack. A comparison of lift and drag for both airfoils concludes that airfoil with tubercles delays stall compared to normal airfoil and has softer stall. Tubercle airfoil maintain high lift coefficients even at high angle of attack. From the flow pattern it is also seen that tubercle airfoil created a number of counter rotating vortices unlike the normal airfoil. The relative strength of vortices on the suction and pressure surface of airfoil depends on the symmetricity of flow

Keywords: Tubercle, Aerodynamic characteristics, flow pattern, counter rotating vortices

1 Introduction

The protuberances on the leading edge of an airfoil capable of altering the fluid flow are called tubercles. The concept of tubercle is inspired from the protuberances seen on the flipper of a Humpback whale [1] as shown in figure 1. The cross of the flipper is similar to a NACA 634-21airfoil and tubercles on the flipper aids in keeping the flow attached to the surface for a wider range of angle of attack and thereby delaying stall. It can be said that tubercles can function as a certain lift enhancement device which increases the maximum lift coefficient without much increase in drag [2]

Figure 1 Humpback whale with tubercles on the flipper (http://www.oceanwideimages.com)

Numerical study on NACA- 63_4-21airfoil modified with tubercle showed an increase in lift and a reduction in induced drag at 10 degree angle of attack [3].Experimental study on NACA 0020 airfoil with tubercle showed a drastic increase in stall angle, reduction of drag in the post stall region and an increase in maximum coefficient of lift when compared to normal NACA 0021airfoil[4].

However, an experimental study done by Stein and Murray [5]using on a sinusoidal leading edge 2D airfoil having amplitude and wavelength similar to that of the flipper on a humpback whale gave a contrary result. They found that the presence of tubercle increased

drag and reduced lift when compared to airfoil with straight leading edge. Another study ny Johari et al also showed that tubercle airfoil has lower A significant study by Murray et.al shows that sweeping of 3D airfoil can give improved aerodynamic characteristics.[6].

Hansen [7] evaluated the aerodynamic characteristics of NACA 0021 and NACA 65021 with varying amplitude and wavelength of the tubercle. It was found that reduction in tubercle amplitude leads to a higher C_{Lmax} and higher stall angle whereas in the post stall regime, performance of larger amplitude tubercles was more favourable. A reduction in wavelength leads to improvements in all aspects of lift performance, including maximum lift coefficient, stall angle, and post stall characteristics.

2. Numerical Analysis

2.1 Airfoil models

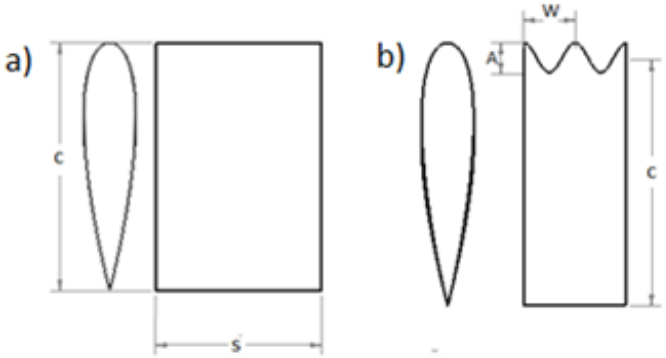

Figure 2:Geometrical parameters for airfoils studied a) normal airfoil b) tubercle airfoil

Two airfoils one with straight leading edge and other with a sinusoidal leading edge are adopted for the study. The geometrical parameters of the airfoil are shown in Figure 2 and further enlisted in table 1. The tubercle and wavelength for the airfoil is selected based on the experimental study done by Hansen et.al., giving best performance.

Table 1:Geometrical parameters of the modelled airfoils

Label	Amplitude, A	Wavelength, W	Mean Chord, c	Span ,S
NACA 0021	N/A	N/A	150 mm	100 mm
NACA 0021 -T	9 mm(0.06 c)	31 m (0.21 c)_	150 mm	62 mm

2.2 Computational domain, grid and boundary conditions

A rectangular domain with structured and hexahedral elements is constructed as the domain of computation as shown in Figure 3.a. Domain is bounded by inlet at 10 chord lengths from the leading edge of airfoil, outlet at 15 chord lengths, farfields at 10 chord lengths on top and bottom. The lateral planes are designated as symmetry. The airfoil is given no slip wall condition.

The structured grid is made using ICEM -CFD. From a mesh sensitivity study, almost 13 lakh elements are used in the numerical analysis of tubercle airfoil. Due to the rather simpler geometry approximately same number of elements are used in normal airfoil also. Figure 3.b and 3.b shown the grid near normal airfoil and tubercle airfoil respectively. The boundary layer close to airfoil wall is resolved with large number of grids such that $y^+=1$ as per requirement of the turbulence model used.

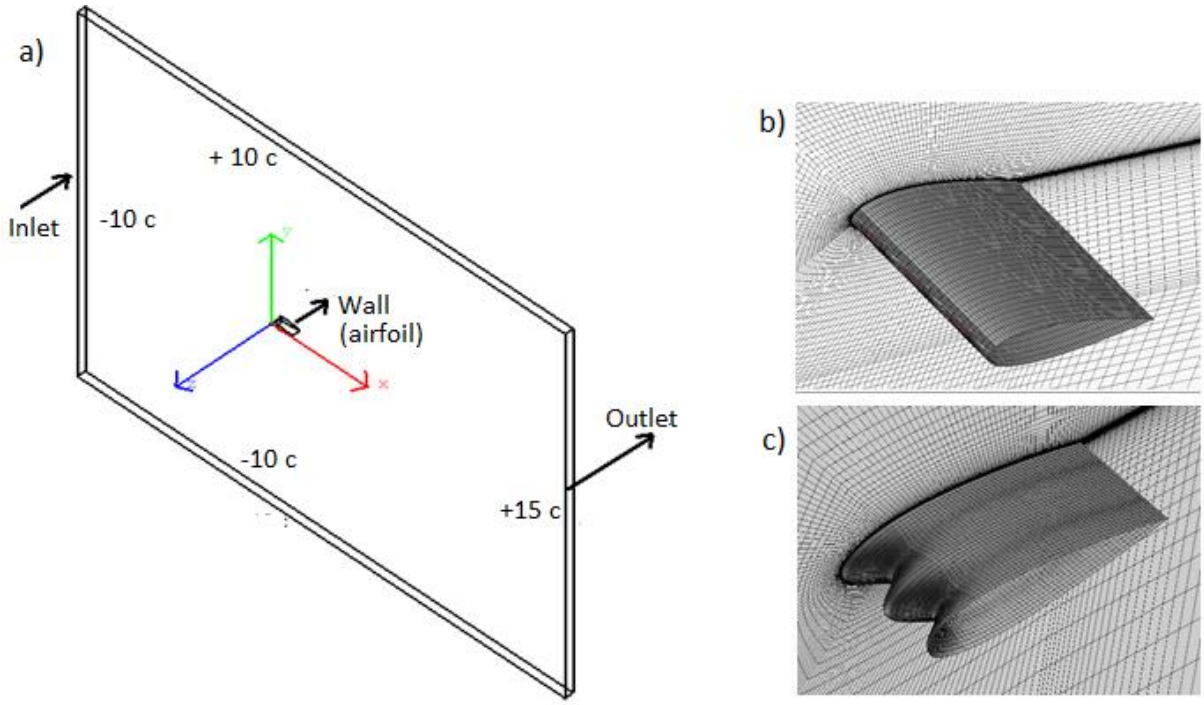

Figure 3. a) Computational domain and boundary conditions b)grid for normal airfoil c) grid for tubercle airfoil

2.3 Turbulence model

Addition to continuity and momentum two more transport equation has to be solved,. The turbulence model used is (shear stress transport) SST $k-\omega$, developed by Menter[9] which is a two equation eddy viscosity model -one for turbulent kinetic energy(k) and one for specific dissipation rate(ω).The transport equations for k and ω are[10] :

$$\frac{\partial}{\partial t}(\rho k)+\frac{\partial}{\partial x_i}(\rho k u_i)=\frac{\partial}{\partial x_j}\left(\Gamma_k\frac{\partial k}{\partial x_j}\right)+\mathrm{G}_k-\mathrm{Y}_k+\mathrm{S}_k \quad (1)$$

$$\frac{\partial}{\partial t}(\rho \omega)+\frac{\partial}{\partial x_i}(\rho \omega u_i)=\frac{\partial}{\partial x_j}\left(\Gamma_\omega\frac{\partial \omega}{\partial x_j}\right)+\mathrm{G}_\omega-\mathrm{Y}_\omega+\mathrm{S}_\omega+\mathrm{D}_\omega \quad (2)$$

The term G_k in equation 1 denotes the turbulent kinetic energy production and is evaluated as $\mathrm{G}_k=\mu_t S^2$so as to be compatible with the Boussinesq hypothesis. Here S is the modulus of the mean rate of strain tensor given by$S\equiv\sqrt{2S_{ij}S_{ij}}$.

The effective diffusivity of k if given by $\Gamma_\mathrm{k}=\mu+\frac{\mu_\mathrm{t}}{\sigma_\mathrm{k}}$. μ_t denotes the turbulent viscosity and is given by $\mu_t=\frac{\rho k}{\omega}\frac{1}{max\left[\frac{1}{\alpha^*},\frac{SF_2}{\alpha_1\omega}\right]}$ and σ_k is the turbulent Prandtl number for k given by $\sigma_k=\frac{1}{\frac{F_1}{\sigma_{k,1}}+\frac{1-F_1}{\sigma_{k,2}}}$

Where,

$F_1 = \tanh(\Phi_1{}^4)$, $F_2 = \tanh(\Phi_2{}^4)$

$$\Phi_1 = min\left[max\left(\frac{\sqrt{k}}{0.09\omega y}, \frac{500\mu}{\rho y^2 \omega}\right), \frac{4\rho k}{\sigma_\omega D_\omega^+ y^2}\right]$$

$$D_\omega^+ = max\left[2\rho \frac{1}{\sigma_{\omega,2}} \frac{1}{\omega} \frac{\partial k}{\partial x_j} \frac{\partial \omega}{\partial x_j}, 10^{-10}\right]$$

$$\Phi_2 = \left[max\left(2\frac{\sqrt{k}}{0.09\omega y}, \frac{500\mu}{\rho y^2 \omega}\right)\right]$$

In the equation 1 ,term Y_k denotes the turbulent kinetic energy dissipation and is evaluated as $Y_k = \rho\beta^* k\omega$

Where

$\beta^* = \beta_i^*[1 + \zeta^* F(M_t)]$,

$\beta_i^* = \beta_\infty^* \left(\frac{\frac{4}{5} + (Re_t/R_\beta)^4}{1 + (Re_t/R_\beta)^4}\right)$

$\zeta^* = 1.5$, $\beta_\infty^* = 0.09$, $R_\beta = 8.$

The compressibility function $F(M_t) = \begin{cases} 0 & M_t \le M_{t0} \\ {M_t}^2 \le {M_{t0}}^2 & M_t > M_{t0} \end{cases}$

Where ${M_t}^2 \equiv \frac{2k}{a^2}$, $M_{t0} = 0.25$, $a = \sqrt{\gamma RT}$

Similarly the term G_ω in equation 2 denotes the ω generation and is evaluated as $G_\omega = \frac{\alpha}{\upsilon_t} G_k$.The coefficient α is given by $\alpha = \frac{\alpha_\infty}{\alpha^*}\left(\frac{\alpha_0 + Re_t/R_\omega}{1 + Re_t/R_\omega}\right)$

$\alpha_\infty = F_1\alpha_{\infty,1} + (1 - F_1)\alpha_{\infty,2}$ where $\alpha_{\infty,1} = \frac{\beta_{i,1}}{\beta_\infty^*} - \frac{\kappa^2}{\sigma_{w,1}\sqrt{\beta_\infty^*}}$ and $\alpha_{\infty,2} = \frac{\beta_{i,2}}{\beta_\infty^*} - \frac{\kappa^2}{\sigma_{w,2}\sqrt{\beta_\infty^*}}$

$R_\omega = 2.95, \quad Re_t = \frac{\rho k}{\mu\omega}, \quad \alpha^* = {\alpha_\infty}^* \left(\frac{{\alpha_0}^* + Re_t/R_k}{1 + Re_t/R_k}\right)$, $R_k = 6$, ${\alpha_0}^* = 0.024$, $\kappa = 0.41$

The effective diffusivity of ω is given by $\Gamma_\omega = \mu + \frac{\mu_t}{\sigma_\omega}$. σ_ω is the turbulent Pandtl number for ω given by $\sigma_\omega = \frac{1}{\frac{F_1}{\sigma_{\omega,1}} + \frac{1 - F_1}{\sigma_{\omega,2}}}$.

In equation 2 , Y_ω denotes the dissipation of ω and is given by $Y_k = \rho\beta\omega^2$

Where $\beta = \beta_i\left[1 - \frac{\beta_i^*}{\beta_i}\zeta^* F(M_t)\right]$ and $\beta_i = F_1\beta_{i,1} + (1 - F_1)\beta_{i,2}$

It is known that SST k omega is a blend of k epsilon and k omega. Thus transformation of k-epsilon model to equations based on k and omega introduces a term D_ω as seen in equation 2 which is defined as $D_\omega = 2(1 - F_1)\rho \frac{1}{\omega\sigma_{\omega,2}} \frac{\partial k}{\partial x_j} \frac{\partial \omega}{\partial x_j}$

The various constants used in SST models are:-

$\sigma_{k,1} = 1.176$, $\sigma_{k,2} = 1$, $\sigma_{\omega,1} = 2$, $\sigma_{\omega,2} = 1.168$, $a_1 = 0.31$, $\beta_{i,1} = 0.075$, $\beta_{i,2} = 0.0828$, $\alpha_\infty^* = 1$, $\alpha_\infty = 0.52$, $\alpha_0 = 1/9$, $\beta_\infty^* = 0/09.$

2.4 Numerical Scheme Validation

The solver and the boundary conditions are validated by comparimg the value of lift coeffient and drag cooefficient obtained from simulation with experimental values[11].. It is obseved that the the coeffient of drag is under predicted in the post stall region which could be the incapability of solver to predict pressure drag caused by flow separation.However, it is seen that there is good agreement of the numerical value with the experimental one.

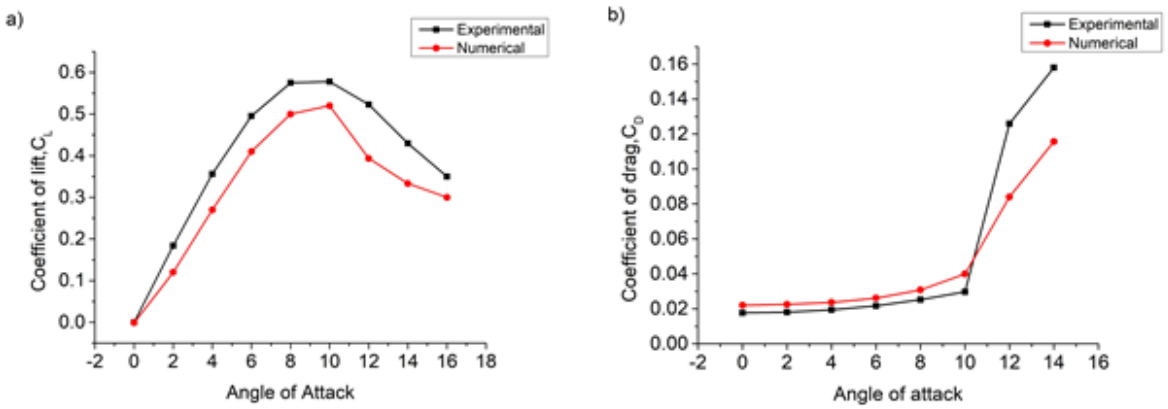

Figure 4 : Comparison of numerical and experimental results of NACA 0021 a) Lift characteristics b)Drag characteristics

3.Results and Discussions

3.1 Lift And Drag

Figure 5.a shows a comparison of lift coefficient at various angle of attacks for a normal unmodified airfoil and a tubercle airfoil. It is seen that the normal airfoil stalls at an angle of attack 10 degree. Beyond 10 degree the lift is decreased drastically showing a steep stall s=characteristic. However in a tubercle airfoil even after 10 degrees, lift is not degraded drastically and there is a soft stall. In the drag characteristics shown in Figure 5.b it is seen that tubercle has no effect at very small angle of attack (0 and 2 degree) but in the pre stall region increases drag. Similar results were obtained in the experimental study done by [3].It can be said that the tubercle airfoil has superior aerodynamic characteristics in the post stall region compared to normal airfoil .

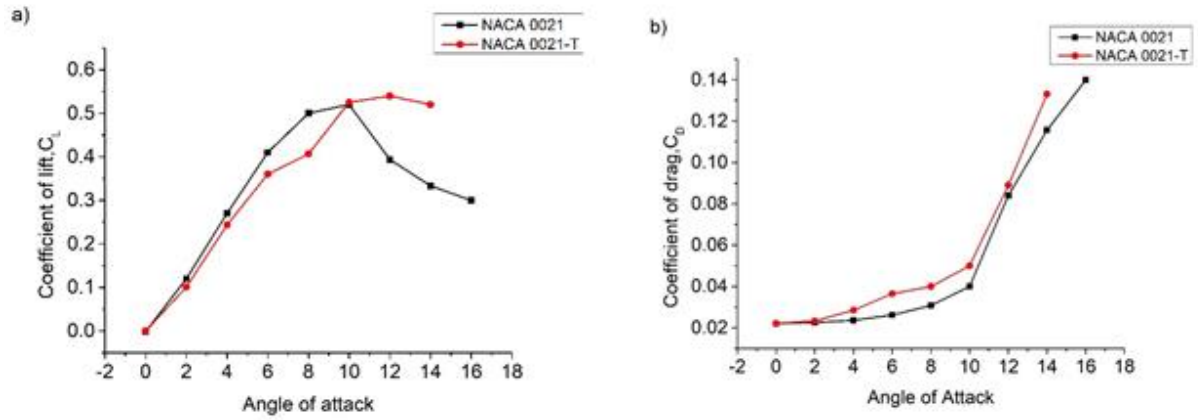

Figure 5: Comparison of normal and tubercle NACA 0021 airfoil a) Lift characteristics b)Drag characteristics

3.2 Velocity streamlines

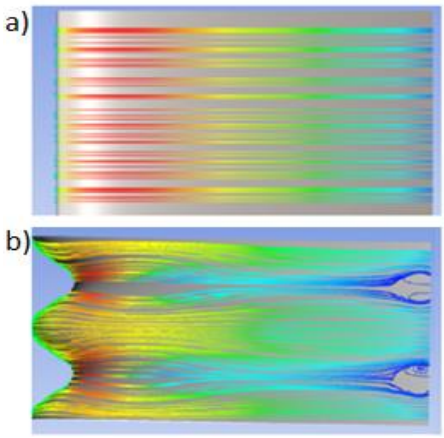

Figure 6:Streamlines on suction surface a) normal airfoil b) tubercle airfoil

Figure 6 shows a comparison of streamlines for both airfoils at 0 dgree angle.As seen in Figure 10.a the flow pass over the airfoil smoothly and leave the trailing edge.However for the tubercle airfoil near the trailing edge the flow is convected around some arbitary point which forms 3D vortices which are counter rotating which will be discused in section 3.3. The changes that occur in streamlines over tubercle airfoil with varying angle of attack is depicted in Figure 7.It is seen that as the the angle of attack increases the flow convection aond arbitary point starts early.This phenomenon is unlikely to happen for a normal airfoil,where as angle of attack increased, flow separates and leave the surface but do not produce counter rotating vortices.

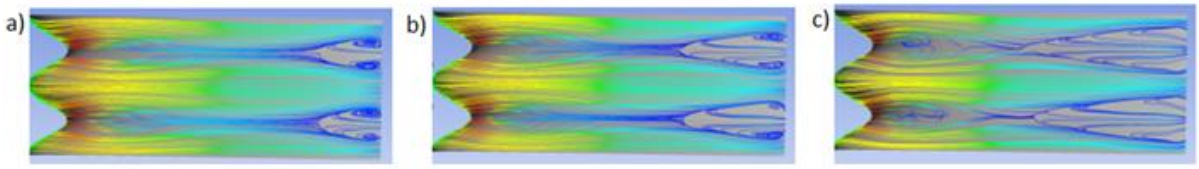

Figure 7: Streamlines on tubercle airfoil a) 2^0 AoA b) 4^0 AoA c) 6^0 AoA

3.3 Stream wise vorticity

To study the contours of streamwise vorticity and turbulent kinetic energy of at the wake region, four planes namely A,B,C and D are chosen at distance 30 mm,90 mm ,150 mm and 250 mm away from the airfoil trailing edge as shown in Figure 8. Figure 9,10 and 11 shows the contours of streamwise vorticity at these planes at 0^0, 4^0, and 6^0.

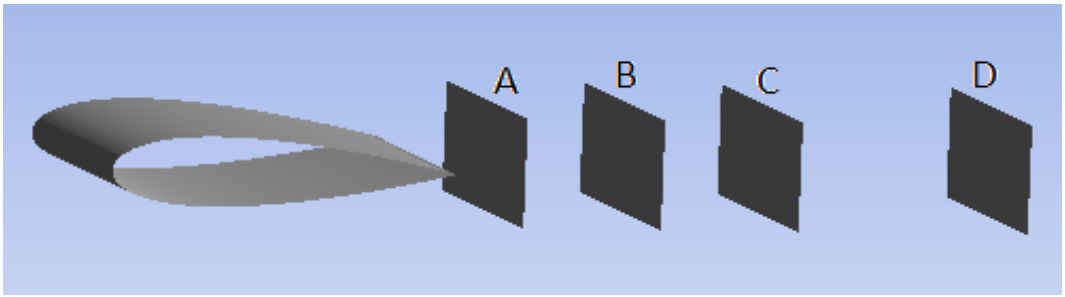

Figure 8: Diagram showing location of planes used for visualization

As seen in figure 9, when the angle of attack is zero there pairs of counter rotating vortices of equal strength are seen on top and bottom side of the airfoil (red colour indicate positive values and therefore clockwise vortex and blue indicate counter clockwise vortex).As we move away in the wake region the vortices are still prominent though it diffused into a larger area .The symmetric nature of vortex can be attributed to the symmetrical flow around the airfoil section(NACA 0021 being a symmetrical airfoil).

However as the angle of attack increases the strength of vortices on the top goes on increasing while it decreases on the bottom side. As the angle of attack reaches 6 degrees the vortices on the bottom side are barely seen

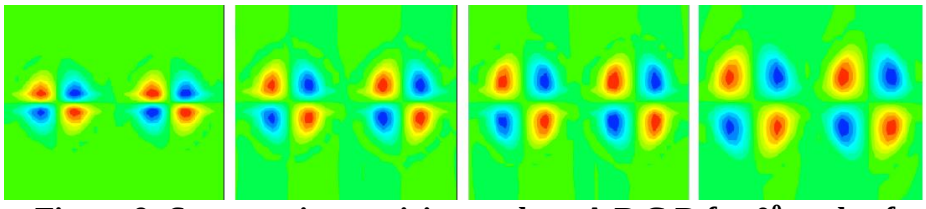

Figure 9: Stream wise vorticity at plane A,B,C,D for 0^0 angle of attack

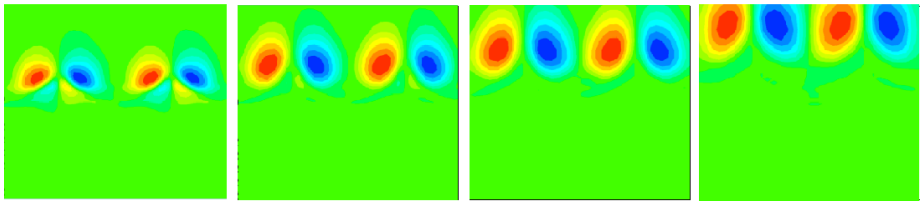

Figure 10:Stream wise vorticity at plane A,B,C,D for 4^0 angle of attack

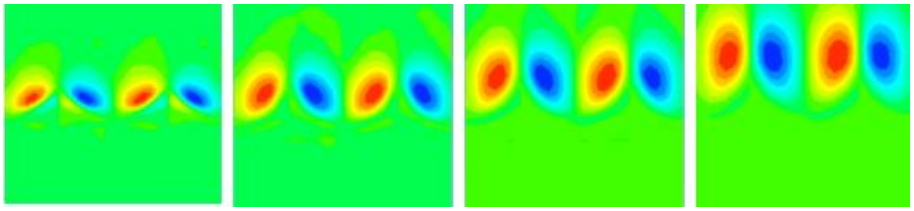

Figure 11:Stream wise vorticity at plane A,B,C,D for 6^0 angle of attack

3.4 Turbulent kinetic energy(TKE)

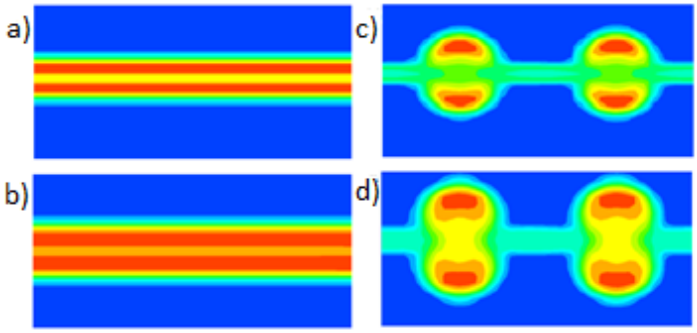

Figure 12:TKE contours at planes A and B for normal and tubercle airfoil

Figure 12.a and 12.c shows the turbulent kinetic energy contours at plane A for normal and tubercle airfoil respectively. It is seen that TKE is distributed uniformly for normal airfoil whereas for tubercle airfoil it is larger in the trough region.

When moving further downstream to plane B the TKE dissipates over larger area.The variation of TKE with change in angle of attack is shown in figure 13.Onset of turbulence happen in trough for all airfoils. As the angle of attack increases the earlier turbulence begins.

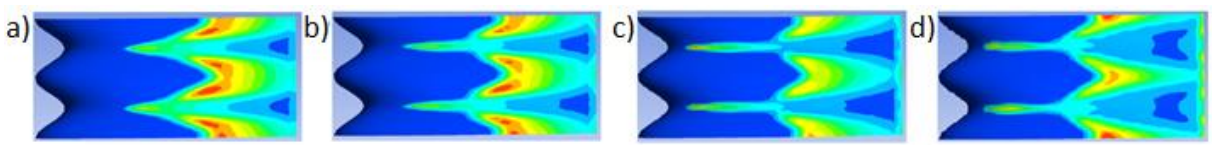

Figure 13:Turbulent kinetic energy on surface of tubercle airfoil a) AoA 0^0 b)AoA 2^0 c)AoA 4^0 d) AoA 6^0

5 Conclusions

A simple modification on the leading edge of an airfoil can drastically alter the flow patter and aerodynamic characteristics. A sinusoidal leading edge on airfoil is seen to have improved the post stall characteristics of NACA 0021 airfoil. The leading edge tubercle creates counter rotating vortices in the trough region which aid in altering the flow pattern.

References

1.Benke, H. (1993). Investigations on the osteology and the functional morphology of the flipper of whales and dolphins (Cetacea). Invest. Cetacea 24, 9-252.

2.Fish, F.E. and Battle, J.M., Hydrodynamic design of the humpback whale flipper, J. Morp., 225:51-60, 1995..

3.Watts, P. and Fish, F.E., The Influence of Passive, Leading Edge Tubercles on Wing Performance, Proc. Of Unmanned Untethered Submersible Technology (UUST), Durham, NH, August, 2001

4.D.S. Miklosovic, M.M. Murray, L.E. Howle, and F.E. Fish: "Leading-edge Tubercles Delay Stall on Humpback Whale (Megaptera novaeangliae) Flippers". Physics of Fluids, Vol. 16, No. 5 (2004).

5 Stein, B. & Murray, M.M., Stall mechanism analysis of humpback whale flipper models, Proc. of Unmanned Untethered Submersible Technology (UUST), Durham, NH, August 2005

6.Murray, M.M., Miklosovic D.S., Fish, F.E., Howle, L.E., Effects of leading edge tubercles on a representative whale flipper model at various sweep angles, Proc.of Unmanned Untethered Submersible Technology (UUST),Durham, NH, August 2005.

7 .Johari, H., Henoch, C., Custodio, D., Levshin, A.: Effects of leading edge protuberances on airfoil performance. AIAA J. **45**(11), 2634–2642 (2007) Kristy L.

8.Hansen, Richard M. Kelso, and Bassam B. Dally: "Performance Variations of Leading-Edge Tubercles for Distinct Airfoil Profiles", AIAA Journal, Vol. 49, No. 1 (2011)

9. Menter, F. R. (1993), "Zonal Two Equation k-ω Turbulence Models for Aerodynamic Flows", AIA A Paper 93-2906

10. Ansys fluent theory guideA Fluent - ANSYS Inc., USA, 2011

11.Sheldahl, R. E., Klimas, P. C., 1981. Aerodynamic characteristics of seven symmetrical airfoil sections through 180-degree angle of attack for use in aerodynamic analysis of vertical axis wind turbines. Sandia National Laboratories

.